JOURNAL OF MATERIALS SCIENCE 37 (2002) 1197–1201

# Processing maps for hot deformation of $\alpha_2$ aluminide alloy Ti-24Al-11Nb

S. V. S. NARAYANA MURTY*, B. NAGESWARA RAO‡
*Materials and Metallurgy Group, ‡Structural Engineering Group, Vikram Sarabhai Space Centre, Trivandrum 695 022, India

B. P. KASHYAP
Department of Metallurgical Engineering and Materials Science, Indian Institute of Technology-Bombay, Mumbai 400 076, India

Using the test data of $\alpha_2$ titanium aluminide alloy Ti-24Al-11Nb with microstructural observations, studies are made to examine the flow localization concepts as well as the simplified metallurgical stability criterion for delineating the regions of flow instabilities in the processing maps. The optimum hot working conditions for the material are suggested.


## 1. Introduction

Deformation processing of titanium alloys is of considerable interest in view of their low density and high temperature capabilities. Ordered intermetallic titanium aluminide alloys based upon the $Ti_3Al$ ($\alpha_2$) and TiAl ($\gamma$) phases are of great interest because of their substantially higher use temperatures as compared to conventional $\alpha$, $\alpha/\beta$ and $\beta$ titanium alloys [1]. As with other titanium alloys, the mechanical properties of these materials are very sensitive to microstructure [2, 3], which led to extensive study of the hot deformation of this material. Semiatin *et al.* [4] and Sagar *et al.* [5] have examined the hot deformation characteristics of Ti-24Al-11Nb alloy in a wide range of temperatures and strain rates.

One of the requirement for forge process modeling is a knowledge of the alloy flow behavior for defining deformation maps that delineate "safe" and "nonsafe" hot working conditions. These maps show in the processing space (that is on axes of temperature and strain rate) the processing conditions for stable and unstable deformation.

Flow localization may occur during hot working in the absence of frictional or chilling effects. In this case, localization results from flow softening (negative strain hardening). Flow softening arises during hot working as a result of structural instabilities such as adiabatic heating, generation of a softer texture during deformation, grain coarsening or spheroidisation. Flow softening has been correlated with material properties by the parameter, for plane strain compression [6–8]:

$$\alpha = \frac{-\gamma}{m} \tag{1}$$

where the normalized flow softening rate,

$$\gamma = \frac{1}{\sigma}\frac{\mathrm{d}\sigma}{\mathrm{d}\varepsilon} = \frac{\partial \ln \sigma}{\partial \varepsilon} \tag{2}$$

and the strain rate sensitivity parameter,

$$m = \frac{\mathrm{d}\log\sigma}{\mathrm{d}\log\dot{\varepsilon}}. \tag{3}$$

Here, $\sigma$, $\varepsilon$, $\dot{\varepsilon}$ and $T$ are the flow stress, strain, strain rate and temperature respectively. Flow localization will occur if the parameter,

$$\alpha > 5 \tag{4}$$

which has been fixed on the basis of microstructural observations in titanium and its alloys.

The mechanical behaviour of materials under processing is generally characterized by one of the following constitutive equations:

$$\sigma = f_\sigma(\varepsilon, \dot{\varepsilon}, T) \tag{5a}$$

or

$$\dot{\varepsilon} = f_{\dot{\varepsilon}}(\varepsilon, \sigma, T). \tag{5b}$$

The stability criterion developed by Murty and Rao [9] is based on the irreversible thermodynamics of large plastic flow proposed by Ziegler [10]. According to the principles of maximum rate of entropy production, a system undergoing large plastic deformation will be unstable if the rate of change in the dissipation function ($D(\dot{\varepsilon})$) with strain rate ($\dot{\varepsilon}$) satisfies the inequality:

$$\frac{\mathrm{d}D}{\mathrm{d}\dot{\varepsilon}} < \frac{D(\dot{\varepsilon})}{\dot{\varepsilon}}. \tag{6}$$

It is well known that during deformation, power dissipation occurs through a temperature rise (termed the $G$ content) and microstructural change (termed $J$ co-content) of the work piece material. In general, most of the dissipation is due to a temperature rise, and only a small amount of energy is dissipated through microstructural changes. The power $P$ (per unit volume)

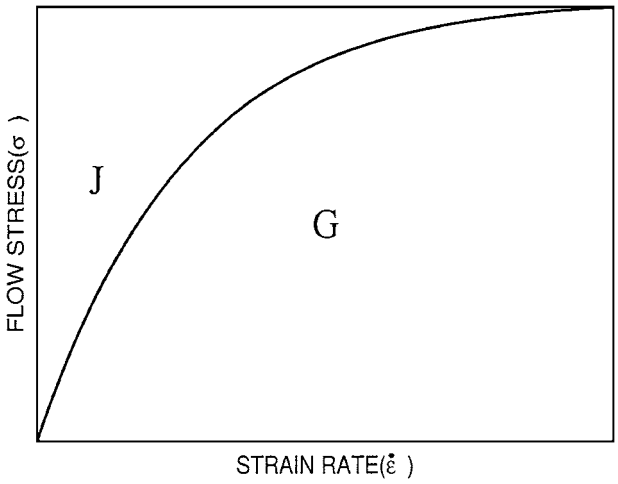


*Figure 1* Schematic representation of stress – strain rate curve showing the areas corresponding to $G$ and $J$.

absorbed by the work piece material during plastic flow is given by

$$P = G + J \tag{7}$$

or

$$\sigma\dot{\varepsilon} = \int_0^{\dot{\varepsilon}} f_\sigma(\varepsilon, \xi, T)\,\mathrm{d}\xi + \int_0^{\sigma} f_{\dot{\varepsilon}}(\varepsilon, \xi, T)\,\mathrm{d}\xi. \tag{8}$$

Fig. 1 shows the stress – strain rate curve of the material showing the areas corresponding to $G$ and $J$.

According to the dynamic material model [11], $D(\dot{\varepsilon})$ is equivalent to $J$ co-content, and the inequality in Equation 6 can be written as

$$\frac{\mathrm{d}J}{\mathrm{d}\dot{\varepsilon}} < \frac{J}{\dot{\varepsilon}}. \tag{9}$$

From Equations 7 and 8,

$$\frac{\partial J}{\partial \dot{\varepsilon}} = \dot{\varepsilon}\,\frac{\mathrm{d}\sigma}{\mathrm{d}\dot{\varepsilon}} = m\sigma. \tag{10}$$

Using Equation 10 in Equation 9, we get

$$m\sigma < \frac{J}{\dot{\varepsilon}}. \tag{11}$$

The efficiency of power dissipation, $\eta$ is given by

$$\eta = \frac{J}{J_{\max}} \tag{12}$$

where

$$J_{\max} = \frac{1}{2}\sigma\dot{\varepsilon} \tag{13}$$

is used to normalize $J$.

From Equations 11–13, the instability condition becomes

$$\eta > 2m. \tag{14}$$

For delineating the regions of flow instability in the processing maps, a simplified condition for stable material flow is

$$0 < \eta < 2m. \tag{15}$$

For the evaluation of $\eta$, it is convenient to write $J$ from Equation 7 in terms of $G$:

$$J = P - G = \sigma\dot{\varepsilon} - \int_0^{\dot{\varepsilon}} f_\sigma(\varepsilon, \xi, T)\,\mathrm{d}\xi$$
$$= \sigma\dot{\varepsilon} - \int_0^{\dot{\varepsilon}} \sigma(\varepsilon, \xi, T)\,\mathrm{d}\xi.$$

Using this expression in Equation 12, the efficiency of power dissipation ($\eta$) can be written in the form:

$$\eta = 2\left[1 - \frac{1}{\sigma\dot{\varepsilon}}\int_0^{\dot{\varepsilon}} \sigma(\varepsilon, \xi, T)\,\mathrm{d}\xi\right]. \tag{16}$$

The second term on the right hand side of Equation 16 indicates the ratio of the average of flow stress distribution up to the strain rate, $\dot{\varepsilon}$ and the flow stress at that strain rate. $\eta$ is a dimensionless parameter and is treated as a workability parameter.

## 2. Generation of workability maps

The test data of Ti-24Al-11Nb presented in Ref. [12] was considered in the present analysis because of its high quality and ability to perform numerical analysis. The data was generated from the hot compression testing of solid cylinders using servohydraulic testing machines capable of imposing constant true strain rates on the specimen. The specimens were compressed to 50% of their initial height and the load-stroke curves obtained were converted in to true stress- true strain curves by subtracting the elastic portion of the strain and using the standard equations for the true stress – true strain calculations. The test data was corrected for the adiabatic temperature rise. One specimen was tested to obtain each result. Table I gives the flow stress values of Ti-24Al-11Nb (having $\beta$ transformed microstructure) at different temperatures and strain rates for various strains. Interpretation of the experimental data for the development of processing maps depends upon the accurate evaluation of the workability parameters, such as the strain rate sensitivity parameter ($m$), the efficiency of power dissipation ($\eta$) and the normalized flow softening rate ($\gamma$).

The test values of $\sigma$ at any $\varepsilon$ and $T$ reported in Tables I and II are for $10^{-3}\ \mathrm{s}^{-1} \le \dot{\varepsilon} \le 10^{2}\ \mathrm{s}^{-1}$, whereas the integration for $G$ in Equation 16 needs the input from $\dot{\varepsilon} = 0$. To overcome this difficulty, the integral in Equation 16 is split as [9]

$$\int_0^{\dot{\varepsilon}} \sigma(\varepsilon, \xi, T)\,\mathrm{d}\xi$$
$$= \int_0^{10^{-3}} \sigma(\varepsilon, \xi, T)\,\mathrm{d}\xi + \int_{10^{-3}}^{\dot{\varepsilon}} \sigma(\varepsilon, \xi, T)\,\mathrm{d}\xi$$
$$= \left[\frac{\sigma(\varepsilon, \dot{\varepsilon}, T)\dot{\varepsilon}}{m+1}\right]_{\dot{\varepsilon}=10^{-3}} + \int_{10^{-3}}^{\dot{\varepsilon}} \sigma(\varepsilon, \xi, T)\,\mathrm{d}\xi. \tag{17}$$

The first term on the right hand side of Equation 17 is evaluated by assuming the power law nature of $\sigma - \dot{\varepsilon}$

TABLE I Flow stress values (in MPa) of Ti-24Al-l1Nb ($\beta$-transformed) at different temperatures and strain rates for various strains (corrected for adiabatic temperature rise) [12]

| Strain, $\varepsilon$ | Strain rate ($s^{-1}$) | Temperature (°C) 900 | 950 | 1000 | 1050 | 1100 |
|---|---|---|---|---|---|---|
| 0.1 | 0.001 | 275.5 | 203.1 | 141.0 | 52.5 | 18.7 |
| | 0.01 | 320.0 | 339.9 | 236.8 | 100.0 | 36.3 |
| | 0.1 | 413.9 | 328.2 | 284.6 | 175.3 | 56.4 |
| | 1.0 | 511.5 | 429.1 | 377.8 | 252.1 | 124.1 |
| | 10.0 | 518.4 | 496.6 | 473.0 | 349.9 | 184.5 |
| | 100.0 | 498.9 | 468.9 | 454.4 | 434.4 | 295.2 |
| 0.2 | 0.001 | 246.0 | 179.4 | 118.9 | 42.5 | 15.9 |
| | 0.01 | 308.3 | 307.5 | 205.0 | 82.4 | 33.7 |
| | 0.1 | 436.6 | 317.5 | 258.5 | 142.5 | 52.2 |
| | 1.0 | 556.1 | 427.2 | 350.8 | 220.5 | 111.1 |
| | 10.0 | 624.3 | 554.4 | 498.3 | 331.9 | 170.6 |
| | 100.0 | 620.0 | 558.9 | 517.5 | 456.9 | 283.1 |
| 0.3 | 0.001 | 220.4 | 159.1 | 105.2 | 37.1 | 14.7 |
| | 0.01 | 291.8 | 275.2 | 186.3 | 74.3 | 32.1 |
| | 0.1 | 435.8 | 301.2 | 234.1 | 122.1 | 47.6 |
| | 1.0 | 561.8 | 413.6 | 324.7 | 201.1 | 102.3 |
| | 10.0 | 637.5 | 549.4 | 481.8 | 301.7 | 148.9 |
| | 100.0 | 659.8 | 588.7 | 529.8 | 447.7 | 263.9 |
| 0.4 | 0.001 | 202.2 | 143.8 | 92.8 | 33.5 | 14.1 |
| | 0.01 | 275.2 | 249.0 | 173.3 | 68.3 | 30.6 |
| | 0.1 | 431.0 | 285.2 | 213.0 | 112.6 | 45.4 |
| | 1.0 | 566.1 | 400.0 | 306.7 | 189.0 | 95.1 |
| | 10.0 | 628.7 | 530.5 | 458.2 | 282.2 | 144.5 |
| | 100.0 | 498.9 | 468.9 | 454.4 | 434.4 | 295.2 |
| 0.5 | 0.001 | 186.8 | 133.6 | 92.8 | 31.5 | 13.8 |
| | 0.01 | 264.8 | 233.7 | 164.3 | 64.8 | 30.0 |
| | 0.1 | 419.9 | 285.2 | 202.1 | 116.1 | 44.9 |
| | 1.0 | 577.9 | 390.4 | 290.2 | 180.4 | 90.9 |
| | 10.0 | 602.0 | 505.8 | 430.4 | 265.6 | 137.2 |
| | 100.0 | 628.4 | 556.1 | 480.9 | 390.3 | 231.1 |

curve:

$$\sigma(\varepsilon, \dot{\varepsilon}, T) = K(\varepsilon, T)\dot{\varepsilon}^m \tag{18}$$

which results

$$\int_0^{10^{-3}} \sigma(\varepsilon, \xi, T)\,\mathrm{d}\xi = \left[\frac{K(\varepsilon, T)\dot{\varepsilon}^{m+1}}{m+1}\right] = \left[\frac{\sigma(\varepsilon, \dot{\varepsilon}, T)\dot{\varepsilon}}{m+1}\right]_{\dot{\varepsilon}=10^{-3}}. \tag{19}$$

The value at $\dot{\varepsilon} = 10^{-3}$ is obtained by finding the slope of $\log(\sigma) - \log(\dot{\varepsilon})$ curve close to the point $\dot{\varepsilon} = 10^{-3}$. A cubic spline fit for the test data is used, to generate a greater number of data points for evaluating the second integral in Equation 17 by trapezoidal rule. Using the determined value of the integral from Equation 17, the efficiency of power dissipation, $\eta$ is obtained from Equation 16. While carrying out the numerical computation, the flow stress data is initially transformed into logarithmic scale, in order to reduce the tenth order magnitude of strain rate to first order to avoid any excessive round off error. With this transformation, the first derivative of the spline fit gives the strain rate sensitivity parameter ($m$) at the generated intermediate data points. The normalized flow softening rate ($\gamma$) is obtained by transforming initially the flow stress data in to a natural logarithmic scale and finding it directly from the first derivative of the spline fit to the data of $\ln\sigma - \varepsilon$ data, at the specified $\dot{\varepsilon}$ and $T$. The value of the workability parameter $\alpha$ is obtained from Equation 1 by substituting the values of $\gamma$ and $m$.

The generation of workability map based on the flow localization concepts of Semiatin and Lahoti [6] (Equation 4) and the instability map based on the simplified metallurgical condition (Equation 15) are explained below.

From Equations 4 and 15, we define the instability parameters for unstable flow as

$$\xi_1 = 1 - \frac{\alpha}{5} < 0 \tag{20}$$

$$\xi_2 = \frac{2m}{\eta} - 1 < 0. \tag{21}$$

The curves represented by $\xi_1 = 0$ and $\xi_2 = 0$ bifurcate the stable and unstable regions in the workability maps for the two criteria considered. The regions where $\xi_1 < 0$ and $\xi_2 < 0$ in the map correspond to unstable flow (microstructural instabilities) in the material. From the determined values of $\alpha$, $m$ and $\eta$, the instability parameters $\xi_1$ and $\xi_2$ defined in Equations 20 and 21 are calculated for the specified value of $\varepsilon$ at different values of $\dot{\varepsilon}$ and $T$. MATLAB (Math Works Inc., USA) software was utilized for generating the two dimensional contour maps.

## 3. Results and discussion

Following the procedure described in the preceding section, the workability maps for the hot deformation of $\alpha_2$ aluminide alloy Ti-24Al-l1Nb in the as cast condition ($\beta$) are generated by using the flow stress data of Table I. Figs 2 and 3 show the contour plots for $\xi_1$ and $\xi_2$ for strains of 0.1, 0.3 and 0.5 superimposed on to each other respectively. In these figures, the regions where $\xi_1 > 0$ and $\xi_2 > 0$ are identified as stable flows and those where $\xi_1 < 0$ and $\xi_2 < 0$ are identified as unstable flows. The condition $m < 0$ is also included for delineating the regimes of instability in Figs 2 and 3. It can be observed from Fig. 2 that the flow is stable in the

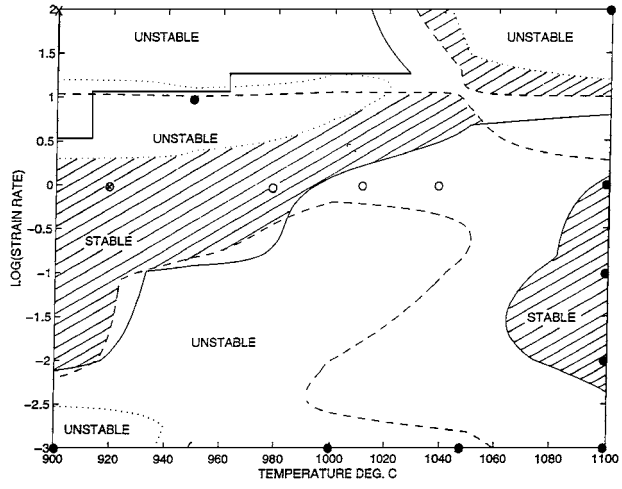


*Figure 2* Contour map based on flow localization concept (Equation 20) at different strains superimposed for Ti-24Al-l1Nb ($\beta$); —— 0.1 - - - - - 0.3; and . . . . . 0.5 with the microstructural observations: ● stable; X unstable [5] and ○ stable; ⊗ unstable [4].

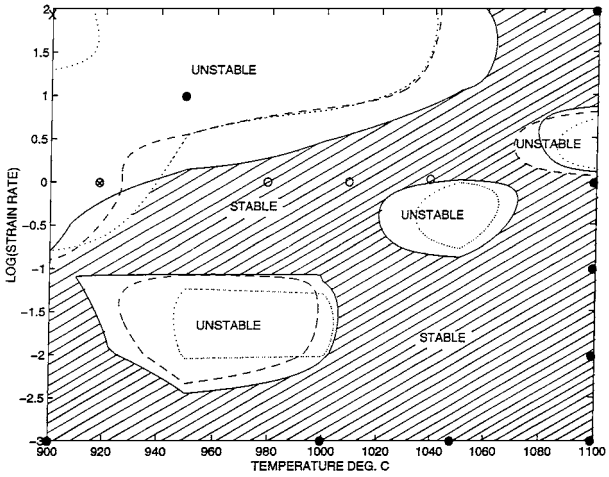


*Figure 3* Contour map of simple instability condition (Equation 21) at different strains superimposed for Ti-24Al-11Nb ($\beta$); —— 0.1 - - - - - 0.3; and . . . . . 0.5 with the microstructural observations: • stable; X unstable [5] and ○ stable ; ⊗ unstable [4].

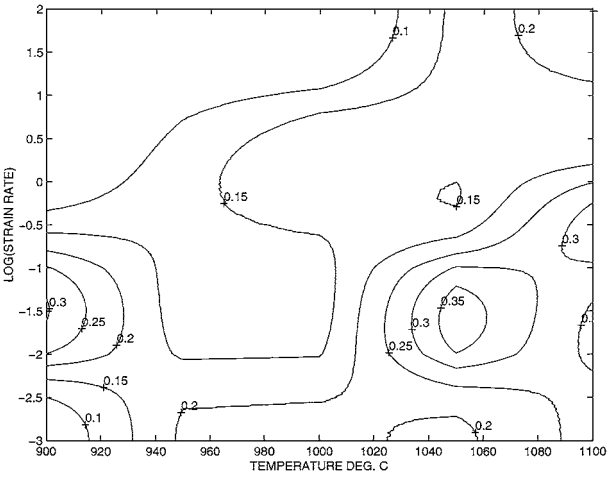


*Figure 4* Contour map for strain rate sensitivity parameter ($m$) for Ti-24Al-11Nb ($\beta$) at a strain of 0.5.

temperature range 1010–1100°C and in the strain rate range 0.001–0.1 $s^{-1}$. It can be noted from Fig. 3 that the condition for unstable flow given by Equation 20 is highly conservative in predicting the regions of unstable flow. Figs 4 and 5 show the contour plots for the strain rate sensitivity parameter ($m$) and the efficiency of power dissipation ($\eta$) at $\varepsilon = 0.5$. For the case of power law stress distribution, the unstable region in the maps will be at those locations where $m < 0$. The maximum value of $m$ in Fig. 4 is found to be 0.382, which occurs at a strain rate of 0.036 $s^{-1}$ ($\log(\dot{\varepsilon}) = -1.44$) and at a temperature of 1050°C . The maximum value of $\eta$ in Fig. 5 is found to be 0.524, which occurs at 1050°C and at a strain rate of 0.068 $s^{-1}$ ($\log(\dot{\varepsilon}) = -1.17$).

It is known from the test results on several materials that the maximization of $\eta$ or $m$ will reduce the tendency for flow localization. At any constant $\varepsilon$ and $T$, the maximum value of $\eta$ with respect to $\dot{\varepsilon}$ becomes $2m/(m+1)$ only when $\partial m/\partial(\ln \dot{\varepsilon}) < 0$. This condition is also verified in the present numerical computation. The microstructural observations of the material presented by Semiatin *et al.* [4] and Sagar *et al.* [5] are marked in Figs 2 and 3. The microstructural observations of the flow instabilities of Ref. [5] are found to be in the marked unsafe regions in Fig. 3 which confirms the validity of the present instability criterion. It should be noted that the condition for unstable flow suggested by Semiatin and Lahoti [5] in Equation 4 has been proposed for titanium and its alloys. In the present case, it is highly conservative in predicting the flow localization. Due to the empirical nature of their criterion, its applicability for other materials will be known only after examining the microstructural instabilities during hot deformation. However, there is no such restriction in the case of simplified stability condition (15). This is because, the condition (15) is based on the continuum principles as applied to large plastic flow as proposed by Ziegler [10]. From the contour maps of $m$ and $\eta$ in Figs 4 and 5, it is preferable to conduct the hot working in the temperature range of 1010–1100 °C and in the strain rate range of 0.001–1.0 $s^{-1}$, at which both $m$ and $\eta$ are maximum.

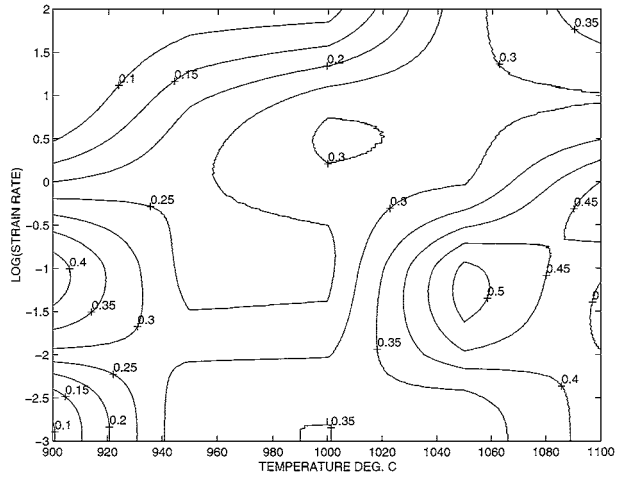


*Figure 5* Contour map for efficiency of power dissipation ($\eta$) for Ti-24Al-11Nb ($\beta$) at a strain of 0.5.

## 4. Concluding remarks

Unstable flow during hot deformation of $\alpha_2$ titanium aluminide alloy Ti-24Al-11Nb was analysed using $\alpha$ parameter as suggested by Semiatin and Lahoti [5] and the simplified metallurgical stability criterion suggested by Murty and Rao [9]. The value of $\alpha$ fixed by Semiatin and Lahoti is based on the microstructural observations on titanium and its alloys. The metallurgical stability condition derived by Murty and Rao [9] based on the continuum principles as applied to large plastic flow, which is not empirical and has no such restrictions has successfully predicted the regions of flow instabilities in the processing maps.

## References

1. H. A. LIPSITT, "High Temperature Ordered Intermetallic Alloys" (MRS, Pittsburgh, PA, 1985) p. 351.
2. C. H. WARD, J. C. WILLIAMS, A. W. THOMPSON, D. G. RASENTHAL and F. H. FROES, *Mem. Etud. Sci. Rev. Metall.* **89** (1989) 647.
3. W. CHO, A. W. THOMPSON and J. C. WILLIAMS, *Met. Trans* A **21A** (1990) 641.
4. S. L. SEMIATIN, K. A. LARK, D. R. BARKER, V. SEETHARAMAN and B. MARQUARDT, *ibid.* **23A** (1992) 295.

5. P. K. SAGAR, D. BANERJEE and Y. V. R. K. PRASAD, *Mat. Sci. & Engg.* A **A177** (1994) 185.
6. S. L. SEMIATIN and G. D. LAHOTI, *Met. Trans* A **13A** (1982) 275.
7. G. E. DIETER, in "Metals Hand Book," 9th ed. Vol. 14 (American Society for Metals, Metals Park, OH, USA, 1988) p. 363.
8. S. L. SEMIATIN and J. J. JONAS, "Formability and Workability of Metals: Plastic Instability and Flow Localization" (American Society for Metals, Metals Park, OH, 1984).
9. S. V. S. NARAYANA MURTY and B. NAGESWARA RAO, *J. Phys. D: Applied Physics* **31** (1998) 3306.
10. H. ZIEGLER, *Progress in Solid Mechanics* **4** (1963) 93.
11. Y. V. R. K. PRASAD, *Indian J. Technology* **28** (1990) 435.
12. Y. V. R. K. PRASAD and S. SASIDHARA, "Hot Working Guide—A Compendium of Processing Maps" (American Society for Metals, Metals Park, OH, 1997).

*Received 22 November 2000*
*and accepted 2 November 2001*